3D Super-virtual Refraction Interferometry

Kai Lu*
King Abdullah University of Science and Technology

ABSTRACT

Super-virtual refraction interferometry enhances the signal-to-noise ratio of far-offset refractions. However, when applied to 3D cases, traditional 2D SVI suffers because the stationary positions of the source-receiver pairs might be any place along the recording plane, not just along a receiver line. Moreover, the effect of enhancing the SNR can be limited because of the limitations in the number of survey lines, irregular line geometries, and azimuthal range of arrivals. We have developed a 3D SVI method to overcome these problems. By integrating along the source or receiver lines, the cross-correlation or the convolution result of a trace pair with the source or receiver at the stationary position can be calculated without the requirement of knowing the stationary locations. In addition, the amplitudes of the cross-correlation and convolution results are largely strengthened by integration, which is helpful to further enhance the SNR. A 3D synthetic example is presented to illustrate the 3D SVI methodology and demonstrate its effectiveness. 3D SVI is also successfully applied to a field data from marine survey, extending the pickable offset from 12 km to at most 18 km.

INTRODUCTION

Traveltime tomography is a widely used tool to estimate the subsurface velocity distribution. Unfortunately, the problem with wide-offset refraction surveys is that the head-wave energy at far offsets can be very weak, which leads to a low SNR of first arrivals. In this case, traveltimes of far-offset traces cannot be accurately picked. To overcome this problem, Bharadwaj and Schuster (2010) and Mallinson et al. (2011) developed the theory of super-virtual refraction interferometry to create head-wave arrivals with much improved SNR.

The traditional SVI is only discussed in 2D cases, where all the refractions from the same layer partly share ray paths, and are called stationary. However, in 3D cases, a pair of refraction traces sharing the same source or receiver can not be guaranteed to be stationary because of the freedom given by the additional dimension in space. In another aspect, the number of source and receiver pairs used to generate a particular head wave, which determines the improvement of the SNR, can be very few when the source and receiver of the targeted trace are at neighboring survey lines. Therefore, applying traditional SVI on 3D cases can be problematic.

This paper proposes a modified 3D SVI method, combining the 2D SVI method with stationary phase integration. Analogous to the application of stationary phase integration on interferometric redatuming (Snieder, 2004), we calculate the cross-correlation or convolution of the stationary trace pair by integrating over the sources and receivers along the survey lines, without the requirement of knowing the locations of stationary sources or receivers. Moreover, this additional integration step also contributes to enhancing the SNR, and thus helps to partly overcome the problems caused by the limitations of the survey geometry.

THEORY

The far-field reciprocity equation of both correlation and convolution types are used to construct super-virtual refractions (Bharadwaj et al., 2011). Figure 1 describes the conventional procedures of creating super-virtual refractions in far-offset traces in 2D media. The assumption is that all the refractions from a certain interface partly share common raypaths. We define a source or receiver stationary if it excites or records refractions sharing common raypaths. In 2D cases, the sources and receivers along the survey line are all stationary.

In 3D seismic survey, it is not straightforward to ap-

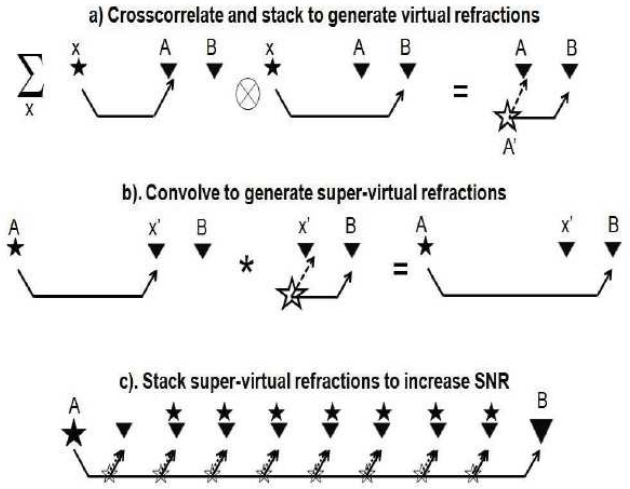

Figure 1: The steps for creating 2D super-virtual refraction arrivals. *a*. Correlation of the recorded trace at A with that at B for a source at x to give the trace $\phi_x(A, B, t)$ with the virtual refraction having traveltime denoted by $\tau_{A'B} - \tau_{A'A}$. This arrival time will be the same for all post-critical source positions, so stacking $\sum_x \phi_x(A, B, t)$ will enhance the SNR of the virtual refraction by $\sqrt{N}$. *b*. Similar to that in a) except the virtual refraction traces are convolved with the actual refraction traces and stacked for different geophone positions to give the *c*. Super-virtual trace with a SNR enhanced by $\sqrt{N}$. Here, N denotes the number of coincident source and receiver positions that are at post-critical offset.

ply the SVI scheme, because the rays are no longer constrained in a plane. For example, the cross-correlation step has to be conducted between two traces sharing a stationary source. In order to pick such two traces, the location of this stationary source needs to be known. However, the stationary source positions are determined not only by the survey geometry, but also by the subsurface structure. Therefore, locating the stationary sources before knowing the subsurface is impracticable. The same problem is with finding the stationary receivers in the convolution step.

I propose a solution to solve this problem by conducting the cross-correlation or convolution step alternatively, avoiding the necessity of locating the stationary sources or receivers. Instead of calculating cross-correlation or convolution using exactly a stationary trace pair, I apply the stationary phase integration (Schuster, 2009) to the source or receiver lines.

The stationary phase analysis (Bleistein, 1984) is introduced here:

$$f(\omega) = \int_{-\infty}^{\infty} g(x) e^{i\omega\phi(x)} dx \sim \alpha g(x^*) e^{i\omega\phi(x^*)}, \qquad (1)$$

where $\phi(x)$ is real and a well-behaved phase function with at most one simple stationary point, ω is the asymptotic frequency, and $g(x)$ is a relatively slowly varying function, $\alpha = e^{i\pi/4}\sqrt{2\pi/(\omega|\phi(x^*)|)''}$ is an asymptotic coefficient, and $x = x^*$ is a stationary point. Equation 1 reveals that, under the far-field approximation, the function $g(x^*)e^{i\omega\phi(x^*)}$ with x^{ast} at the stationary position is kinematically approximated by an integration of this function over all the positions x, if the amplitude is ignored. The stationary position x^* does not have to be known.

Correlation type in 3D SVI

Figure 2 illustrates how stationary phase integration can be applied to the correlation-reciprocity type in SVI. Let $G(A|S) = e^{i\omega\tau_{SA}}$ and $G(B|S) = e^{i\omega\tau_{SB}}$ approximate the normalized refraction waves as shown in Figure 2(a), where $G(A|S)$ and $G(B|S)$ represent the Green's functions originated from the source location S and received at the receiver locations A and B, respectively, and τ_{SA} and τ_{SB} are the traveltimes of refraction SA and SB. In the following, we keep using the notation τ as the traveltime of a refracion, and the subscripts stand for the source and receiver associated with the refraction. Replacing $g(x)e^{i\omega\phi(x)}$ in equation 1 with $G(A|S)\bar{G}(B|S)$ gives the formula

$$\int_{S_1}^{S_n} G(A|S)\bar{G}(B|S)dS = \int_{S_1}^{S_n} e^{i\omega(\tau_{SA}-\tau_{SB})}dS \sim \alpha_1 e^{i\omega(\tau_{S^*A}-\tau_{S^*B})} = \alpha_1 G(A|S^*)\bar{G}(B|S^*), \qquad (2)$$

where $\bar{G}$ represents the complex conjugate of G, S^* denotes the stationary source position, and α_1 is a coefficient. The phase $\phi(S) = \tau_{SA} - \tau_{SB}$ is a function of the

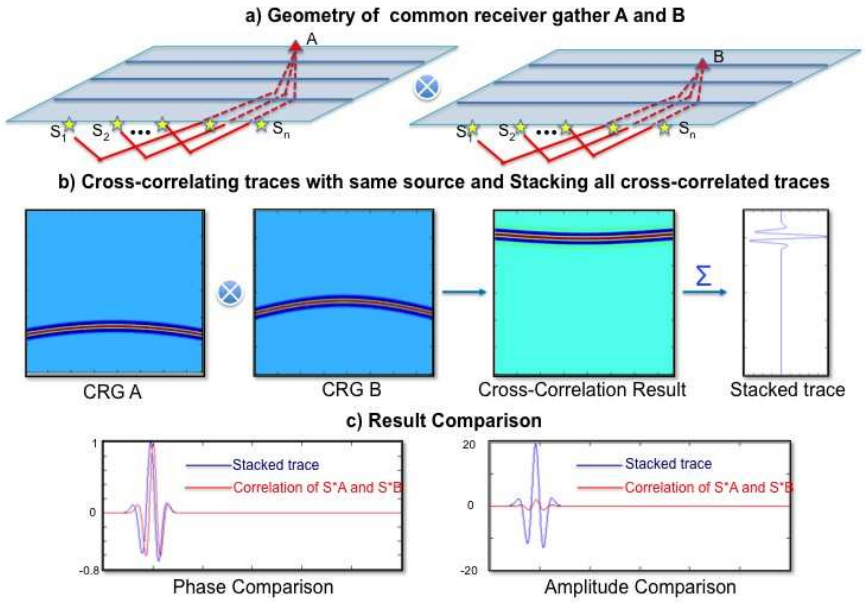

Figure 2: Illustration for creating a virtual trace in 3D with stationary phase integration. a) The geometry of receivers A and B, and the selected source line for integration. b) CRG A and CRG B show the refractions from the same horizontal layer. Every trace in CRG A is cross-correlated with the trace sharing the same source in CRG B. c) All the traces after cross-correlation are stacked to generate the virtual trace AB. The virtual trace generated by integration is compared with that generated by cross-correlating refraction S^*A and S^*B, where S^* is the stationary source location. The stacked virtual trace has an accurate traveltime and much strengthened amplitude.

source location S. The first line in equation 2 is the summation of cross-correlations between refraction SA and SB with different S along the source line, and the second line represents a coefficient multiplying the virtual refraction AB as mentioned in Figure 1, which is calculated by cross-correlating the trace pair $G(A|S^*)$ and $G(B|S^*)$. Equation 2 kinematically calculates the virtual trace AB by stationary phase integration along the source line without knowing the exact location of the stationary source.

Figure 2 is an example illustrating how to create a virtual refraction AB in 3D by the proposed method. Two receivers A and B are fixed and a source line is picked as shown in Figure 2 (a). The raw refraction data of the common receiver gathers (CRG) A and B are shown in the first two pictures of Figure 2 (b). For each source S_i on the source line, a cross-correlation between $G(A|S_i)$ and $G(B|S_i)$ is calculated, where i is the source index from 1 to n, and the result is shown in the third picture of Figure 2(b). The fourth picture is the stacked trace using all the traces from the third picture, which is a numerical implementation result of the first line of equation 2 in the time domain.

In order to test the proposed method, a comparison is shown in Figure 2(c) between the stacked trace, which is the virtual refraction AB calculated by the stationary phase integral method, and the exact virtual refraction AB generated by cross-correlating trace $G(A|S^*)$ and $G(B|S^*)$; here the stationary source S^* is known in the synthetic test. The left-hand-side figure compares the two traces after the normalization, showing that the phase matches well, while the wavelet is a little distorted due to the error coming from the approximation made in equation 2. The right-hand-side figure compares the amplitudes of the two traces. The amplitude of the stacked trace is much stronger than the exact virtual refraction AB, indicating that this integration amplifies the energy of the virtual refraction AB, and also enhances the SNR. Comparing to the 2D SVI workflow, the work introduced so far of generating virtual trace AB in 3D SVI plays the same role as the first step shown in Figure 1 (a), nevertheless with an extra integration.

In 2D SVI, a summation of virtual refraction AB over different source locations x along the survey line as shown in Figure 1 (b) is the key step to increase the SNR. A similar summation is also conducted in 3D SVI as illustrated in Figure 3(a), however, over different source lines instead. Noticing that equation 2 is satisfied regardless which source line is selected, therefore each source line could be picked to produce an equivalent virtual refraction AB by the stationary phase integration. Stacking these virtual refractions generates one with much improved SNR.

Convolution type in 3D SVI

In 2D SVI, A far-offset super-virtual refraction is constructed by convolving a short-offset refraction with the virtual refraction created in the previous correlation step as shown in Figure 1(b). The receiver of the short-offset refraction has to be at the stationary position, which means

the the short-offset refraction and the far-offset super-virtual refraction partly share the common raypath. In a similar way to the previous section, stationary phase integration is applied to calculate the super-virtual refraction in 3D without the knowledge of the stationary receiver locations. Let $G(A|B)^{virt} = e^{i\omega(\tau_{S_BA} - \tau_{S_BB})}$ denote the normalized virtual traces calculated in the previous step, where the receiver A is fixed, receiver B could be any one in the receiver line as shown in Figure 3(b). and S_B is the stationary source location associated with a certain receiver B. Applying equation 1 along the receiver line,

$$\int_{B_1}^{B_n} G(B|S)G(A|B)^{virt}dB = \int_{B_1}^{B_n} e^{i\omega[\tau_{SB}+(\tau_{S_BA}-\tau_{S_BB})]} \sim \alpha_2 e^{i\omega[\tau_{SB^*}+(\tau_{S_{B^*}A}-\tau_{S_{B^*}B^*}))]} = \alpha_2 G(B^*|S)G(A|B^*)^{virt}, \tag{3}$$

where B^* is the stationary receiver associated with the given source S and receiver A, and α_2 is the coefficient. Recognizing that S_{B^*} is actually the given source S in Figure 3(b), equation 3 becomes

$$\int_{B_1}^{B_n} G(B|S)G(A|B)^{virt}dB \sim \alpha_2 e^{i\omega\tau_{SA}} = \alpha_2 G(A|S)^{sv}, \tag{4}$$

where $G(A|S)^{sv}$ is the reconstructed far-offset super-virtual refraction.

The physical interpretation of equation 4 is that the far-offset refraction SA in 3D is kinematically reconstructed by integrating the convolution, which is between the raw refraction data $G(B|S)$ and the pre-calculated virtual refraction $G(A|B)^{virt}$, over the receiver line.

In order to enhance the SNR of the super-virtual refraction SA, a similar stacking to 2D SVI (see Figure 1) is also required. Noticing that equation 4 is satisfied regardless which receiver line is selected, therefore each receiver line could be picked to construct an equivalent super-virtual refraction SA. Figure 3(b) illustrates that stacking these equivalent super-virtual refractions results in a refraction SA with improved SNR.

Workflow

Below is the workflow for 3D super-virtual refraction interferometry:

1. Preprocess the raw data to eliminate some noise, which is helpful for recognizing the target refraction.
2. Properly window the data around the target refraction.
3. Generate the stationary virtual traces by cross-correlation and integrating along a source line.
4. Stack the virtual traces generated from different source lines as shown in Figure 3(a).
5. Generate the stationary super-virtual traces by convolution and integrating along a receiver line.

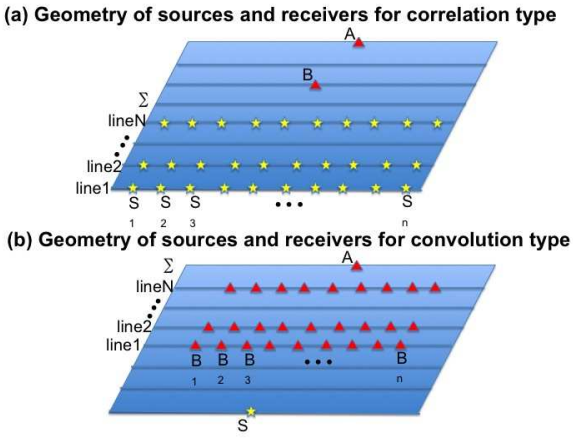

Figure 3: The geometry of sources and receivers for correlation type and convolution type. (a) Virtual traces AB generated with different source lines from line1 to line$N$ are stacked. (b) Super-virtual traces SA generated with different receiver lines from line1 to line$N$ are stacked.

6. Stack the super-virtual traces generated from different receiver lines as shown in Figure 3(b).

The first and second steps in the workflow play an important role in the success of SVI. An ideal window does not contain any other strong coherent events, except for the targeted refraction, in order to avoid strong artifacts from the interferences between unwanted events. Preprocessing the raw data is necessary when the data quality is too low such that the first arrival could not be recognized by raw eyes, and the proper windows could not be picked.

Itetrative SVI

SVI improves the SNR of the data, while the SVI data might be still not clear enough to be easily picked when the background noise is extremely strong. A similar iterative approach as mentioned in 2D SVI (Al-Hagan et al., 2011) could also be applied to 3D cases. The SVI data are used as the input for the next iteration to further improve the data SNR. However, the number of iterations is not unlimited, because each SVI iteration produces artifacts and causes wavelet distortions, therefore too many iterations will deteriorate the data.

NUMERICAL RESULTS

Synthetic Data Example

The proposed method is tested on the synthetic data to demonstrate its effectiveness. Figure 4 shows a 3D undulating two-layer model with the velocity 1500m/s and 3000m/s respectively. The geometry has 11 survey lines on the surface, with 76 shots and 301 receivers in each line.

A common shot gather is shown in Figure 5(a), with the source located at the left end of Line 1, and the receivers

at line N. The first arrivals of the far-offset traces are impossible to pick after strong random noise being added to the synthetic data as shown in Figure 5(b). 3D SVI are applied to the noisy data, and the super-virtual data are shown in Figure 5(c). Compared to the input shown in Figure 5(b), the SVI output shown in Figure 5(c) has the correct traveltimes and much improved SNR. Figure 5(d) shows the iterative SVI data after 2 iterations, in which the SNR is further enhanced compared to Figure 5(c), and the traveltime of the targeted refraction can be easily picked. Figure 6 is the zoom view of the region within the dashed red box in Figure 5. Wavelet distortions are observed from Figure 5 (a), (c) and (d) due to the correlation and convolution operation, therefore a shift should be applied to align the traveltime between the raw pick and SVI pick.

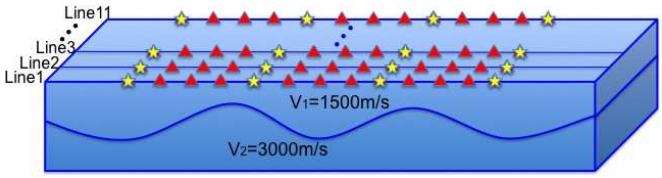

Figure 4: The undulating layer velocity model for synthetic test. 11 survey lines are placed on the ground, with 76 sources and 301 receivers in each line.

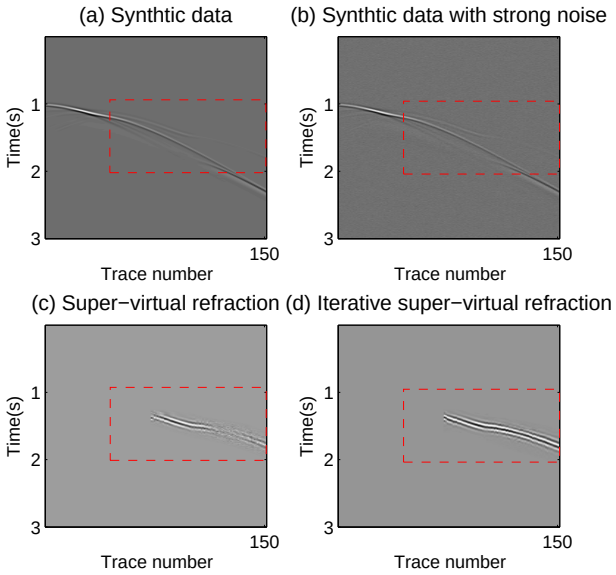

Figure 5: a) The raw common shot gather. b) Strong random noise is added to (a). c) The super-virtual refraction. d) Iterative super-virtual refraction.

Field Data Example

In this section, the proposed method is applied to a 3D OBS field data recorded in the Gulf of Mexico. The survey

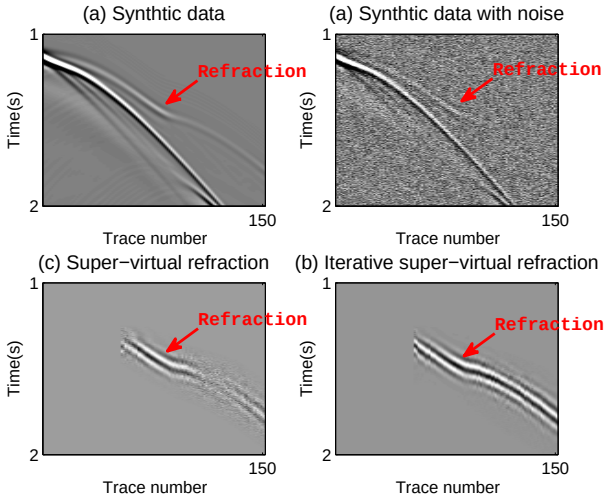

Figure 6: Zoom views of the red boxes in Figure 5.

geometry is shown in Figure 7. The black dots represent recorders installed at the ocean bottom with the depth about 45 m. There are in total 9 OBS lines, and 26 stations in every line with a spacing of approximately 400 m. The green lines represent 153 sail lines, with 360 shots excited along every sail line with a shot interval of 50 m.

Before applying the SVI scheme to the data, a quick scanning of the whole dataset is required. All the data are sorted into several groups, each representing a category of data, in which the first arrivals are refractions from the same layer interface. Each data group is windowed for first arrivals, and processed using SVI workflow separately, to avoid artifacts produced by the interferences between different refraction events. Theoretically, the windowed data don't have to be the first arrivals as long as they can be recognized as the same refraction event. However, a later arrival in the real cases is usually interfered with other coherent events, such as reflections or refractions from different layers, which could bring severe noise and strong artifacts to the SVI result.

A common OBS gather associated with one sail line is extracted as an example here. The location of the OBS station is at the red star and the sources are at the red line marked in Figure 7. Figure 8(a) is the raw data, and the red lines mark two targeted refractions as the first arrivals at medium and far offset. For the convenience in windowing a specific refraction, a 5-15 Hz band-pass filter is applied to suppress the high-frequency noise as shown in Figure 8(b). The SVI scheme is applied to these two refractions individually. Figure 8(c) shows the SNR of both first arrival refractions are improved. The zoom view in Figure 9 shows a detailed comparison between the data before and after SVI. The SVI data are constructed at the correct position with a higher SNR that could be easily picked.

Figure 10 illustrates another data example with a weak far-offset first arrival. The event pointed by the red arrow

is the targeted refraction to be processed. The raw data are preprocessed by a band-pass filter, and the SVI data are normalized trace by trace and plotted in Figure 10(b). The SVI data extend the pickable range to the medium offset, while the most far-offset first arrival is still weak. Iterative SVI with one more iteration is applied to this data to further improve the data SNR as shown in Figure 10, extending the pickable offset from 12km to as far as 18km. A zoom view comparison is shown in Figure 11. Iterative SVI improves the data SNR, nevertheless the wavelet is more distorted. In order to determine the correct traveltime to pick in the SVI data, we first pick the trustworthy part in the raw data as marked by the red solid line in Figure 11 (a). This red line acts as a sign in the SVI data, and could be extended for more picks following the events to the far offset as shown by the dashed line in Figures 11 (b) and (c).

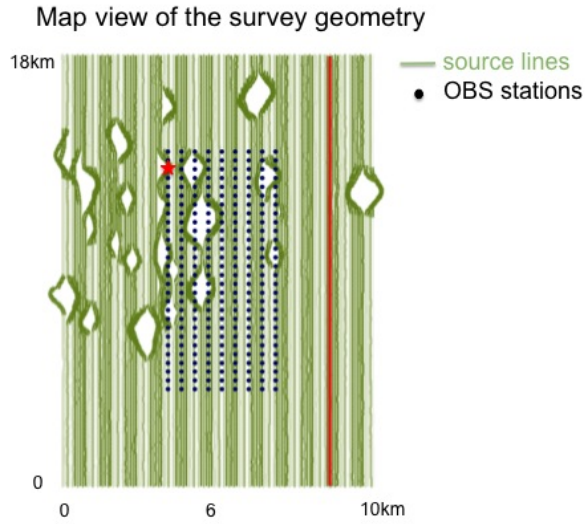

Figure 7: The map view of the survey geometry. The data example shown in the following is an OBS gather with the OBS station located at the red star, and the receivers located at the red line.

DISCUSSION AND CONCLUSION

We introduced the theory of 3D super-virtual interferometry, followed by both synthetic and field examples. The stationary phase integration method is applied with the benefits of avoiding locating the stationary sources and receivers, and further enhancing the SNR. Compared to 2D SVI, two more extra stackings are required on the inline dimension, which dramatically increase both the work amount of windowing first arrivals and the cost of correlation and convolution computation. To reduce the amount of work, especially for a large scale 3D dataset, the range of the stationary phase integration could be shrunk into the Fresnel zone as shown in Figure 12, instead of the whole scale. The contribution from the data out of the Fresnel zone to the integration is minor, and could be neglected.

In practice, the SVI capacity of enhancing the SNR is determined by the number of traces available for stacking, which could be limited due to the geometry. As shown in Figure 12, to create a virtual trace AB, not all the sources are available for the correlation step, but only the ones within the dashed circle, where both the targeted refractions SA and SB are first arrivals. The refractions excited at the source locations out of the dashed circle are later arrivals in the data, and are usually not available for SVI. In this case, the SNR enhancement could be very limited for certain refraction if the dashed circle associated with this refraction only covers a tiny area.

The correlation and convolution operations distort the wavelet of the SVI data, which could be observed in both the synthetic and field data examples. Therefore a shift needs to be added to the SVI traveltime pick. The shift can be calculated by comparing the raw picks and SVI picks at their overlapping offset. The iterative SVI further distorts the wavelet, and usually no more than two iterations is recommended.

ACKNOWLEDGMENTS

The research is supported by funding from King Abdullah University of Science and Technology (KAUST). We thank the CSIM members for supporting this research, and we also thank the High Performance Computational Center and IT support at KAUST. We thank Pemex for providing the GOM field data and giving us the permission to use the data.

REFERENCES

Al-Hagan, O., G. Schuster, and S. Hanafy, 2011, Iterative super-virtual refraction interferometry: CSIM Annual Report, 215–222.

Bharadwaj, P., and G. T. Schuster, 2010, Extending the aperture and increasing the signal-to-noise ratioof refraction surveys with super-virtual interferometry: AGU Annual Meeting Abstracts.

Bharadwaj, P., G. T. Schuster, and I. Mallinson, 2011, Theory of supervirtual refraction interferometry: Geophysical Journal International, **288**, 263–273.

Bleistein, N., 1984, Mathenatical methods for wave phenomena: Academic Press Inc.

Mallinson, I., P. Bharadwaj, G. Schuster, and H. Jakubowicz, 2011, Enhanced refractor imaging by supervirtual interferometry: The Leading Edge, **30**, 546–550.

Schuster, G. T., 2009, Seismic interferomrtry: Cambridge University Press.

Snieder, R., 2004, Extracting the Green's function from the correlation of coda waves, an alternative derivation based on stationary phase: Physical Review E, **69**, 046610.

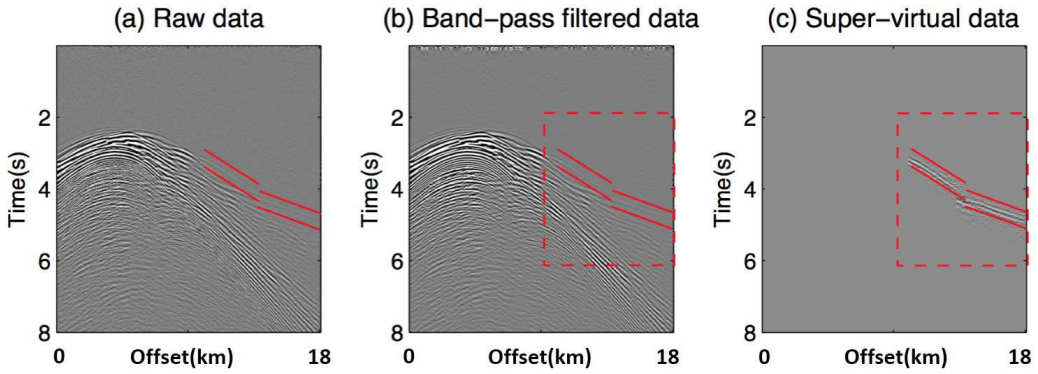

Figure 8: Field data example 1. (a)Raw data, (b) 5-15Hz band-pass filtered data and (c) The super-virtual data.

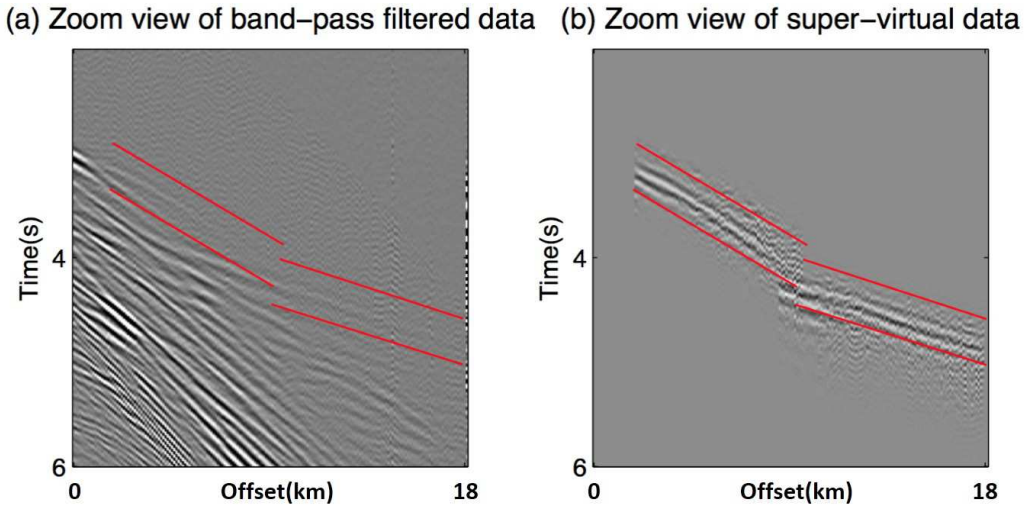

Figure 9: Zoom views of the red boxes in Figure 8 of (a) the band-pass filtered data, (b) the super-virtual data and (c) Iterative super-virtual data.

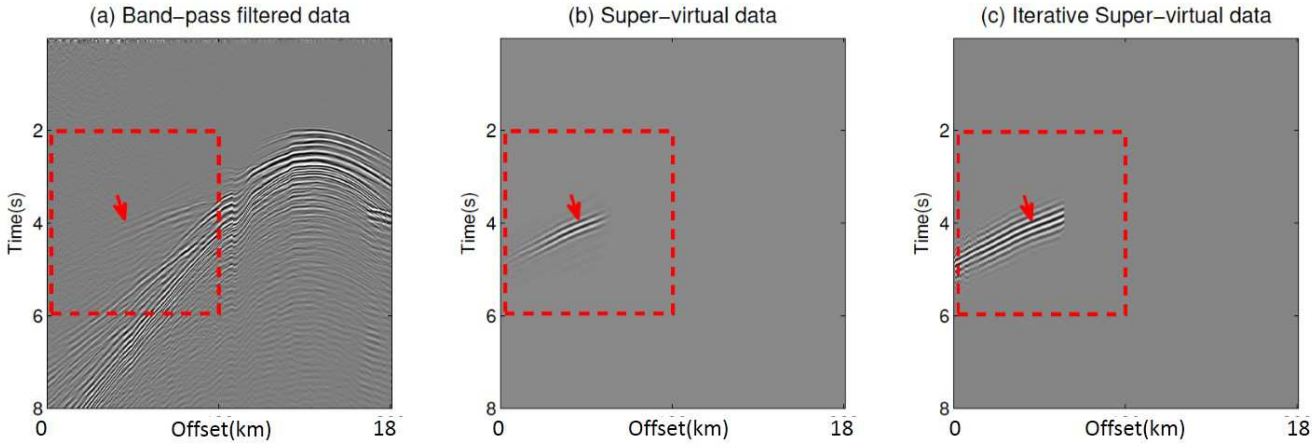

Figure 10: Field data example 2. (a) 5-15Hz band-pass filtered data, (b) The super-virtual data and (c) Iterative super-virtual data

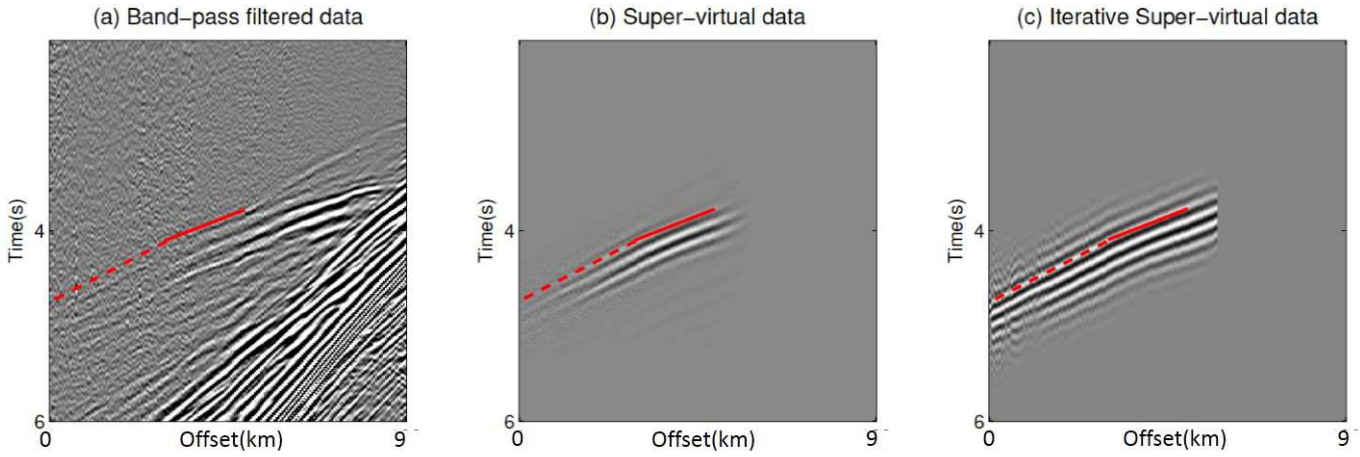

Figure 11: Zoom views of the red boxes in Figure 10 of (a) the band-pass filtered data, (b) the super-virtual data and (c) Iterative super-virtual data. The red lines represent the traveltime picks, and the dashed part denotes the unpickable range before SVI.

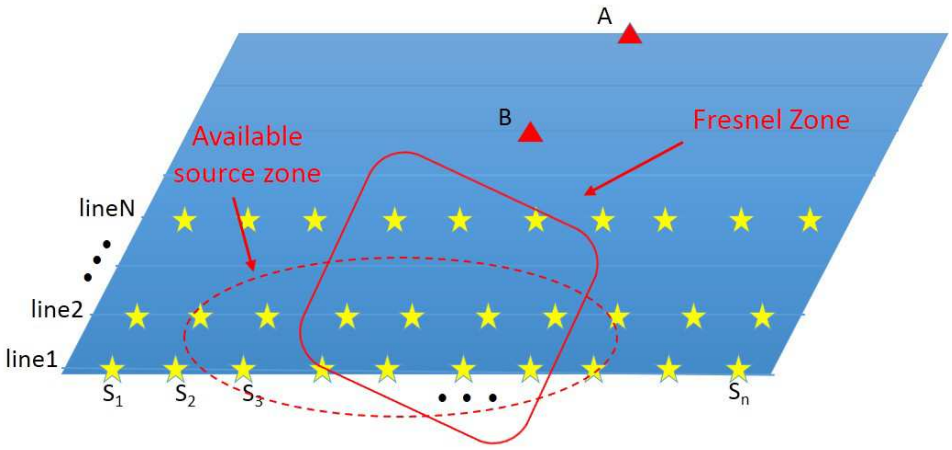

Figure 12: Illustration of the source geometry of creating a virtual trace for two given receivers A and B. The dashed circle denotes the Fresnel zone, within which, the data make the major contribution to the stationary phase integration. The dashed circle denotes an area, within which, for all the sources S, certain targeted refraction event SA and SB are both first arrivals.